PROGRESS IN PHOTOVOLTAICS: RESEARCH AND APPLICATIONS, VOL 2, 3–17 (1994)

Research

Decreased Emitter Sheet Resistivity Loss in High-efficiency Silicon Solar Cells

Armin G. Aberle, Stuart R. Wenham and Martin A. Green

Centre for Photovoltaic Devices and Systems, University of New South Wales, P.O. Box 1, Kensington 2033, Australia

Gernot Heiser

School of Computer Science and Engineering, University of New South Wales, P.O. Box 1, Kensington 2033, Australia

State-of-the-art two-dimensional (2D) numerical semiconductor device simulation tools are applied to bifacially contacted silicon solar cells of practical dimensions in order to investigate the 2D effects arising from ohmic voltage drops in cell emitters due to finite front metal grid line spacings. The 2D simulations show that for typical front finger spacings of high-efficiency silicon solar cells the minority carrier flow in the base deviates strongly from the purely linear flow assumed by one-dimensional (1D) theory. Compared to conventional 1D theory, this 2D effect results in reduced emitter sheet resistivity losses, an increased optimum front finger spacing and a reduced impact of finger spacing on cell efficiency. The 2D effects are of particular importance for concentrator solar cells.

The 2D simulations presented in this work considerably improve the general understanding of internal device physics of high-efficiency silicon solar cells and reveal the limits of 1D models for the simulation of these devices.

INTRODUCTION

Metal electrodes of solar cells are impenetrable for sunlight. In order to allow most of the incident light to enter the device, the front electrode of a conventional solar cell (i.e. a cell with bifacial metal contacts and a full-area current-collecting emitter along the illuminated front surface) consists of a comb-like metal grid. A direct consequence of this grid design is a *lateral* majority carrier flow in the emitter. As emitters of practical silicon solar cells are very thin ($\leqslant 1$ μm), the emitter layer represents a relatively large resistance for this lateral current. Obviously, for small ohmic losses, the emitter should be heavily doped and the metal fingers closely spaced. However, progress in the last decade has shown that this concept is clearly incompatible with high efficiencies of silicon solar cells.[1–3] Heavy doping reduces the open-circuit voltage and the short-circuit current of the cells due to the formation of an emitter layer with poor electronic properties, while closely spaced front fingers result in excessively large shading losses. Consequently, emitters of modern silicon solar cells are lightly doped

1062–7995/94/010003–15 $12.50

Received 8 April 1993
Revised 12 July 1993

and covered by narrow metal fingers spaced as widely as possible without generating excessive emitter ohmic losses. This design provides the best trade-off between the electrical parameters, the open-circuit voltage, short-circuit current and fill factor, which determine the energy conversion efficiency of the cell. The approach generates high open-circuit voltages and short-circuit currents, while the fill factor is below its ideal value owing to finite emitter sheet resistivity losses.

In the past, one-dimensional (1D) models have been widely used to determine the design parameters of silicon solar cells that provide the optimum trade-off between recombination losses, shading losses and resistive losses. In order to approximate the emitter sheet resistivity losses—which are an inherently multi-dimensional effect—1D models assume a spatially constant light-generated minority carrier flow from the base into the emitter. For solar cells with closely spaced front fingers and high emitter sheet conductivity, this method will generally produce accurate results, as two-dimensional (2D) effects in the base of the cells are negligible.

In state-of-the-art silicon solar cells, however, the situation is more complex. To a degree that depends on finger spacing and emitter sheet resistivity, a voltage drop builds up along the emitter surface when a current is generated by the cell. This voltage drop makes the central emitter regions more strongly forward-biased than regions closer to the contact. This increases the minority carrier concentration in the central base region and distorts current flow, as indicated schematically in Figure 1. One-dimensional solar cell theory—which does not take this effect into account—overestimates the resulting lateral current in the emitter, and hence the resistive emitter losses. Therefore, if the effects illustrated in Figure 1 are significant in practical silicon solar cells, the spacing between the front metal fingers can be increased above the limits predicted by 1D theory, and cell efficiency should increase due to reduced shading and metal contact recombination losses.

This paper for the first time quantitatively determines the impact of the 2D effects illustrated in Figure 1 on resistive losses in silicon solar cells. The 2D simulations are performed with the numerical semiconductor device simulator Simul, which has recently been developed at the Swiss Federal Institute of Technology (ETH), Zurich, and allows for the modelling of silicon and GaAs devices in one, two and three dimensions.[4,5]

In the next section the 1D approach, which allows for an approximate determination of the impacts of front finger spacing and emitter sheet resistivity on solar cell I–V characteristics, is described. The principal difficulties encountered in 2D numerical simulations of silicon solar cells are also discussed and the main features of the software package Simul are summarized. The minority carrier flow in the base of high-efficiency silicon solar cells at maximum power point operating conditions is investigated for various illumination spectrums. The 2D simulations reveal that the minority carrier flow in the base deviates strongly from 1D theory and that 1D models overestimate the emitter sheet resistivity losses.

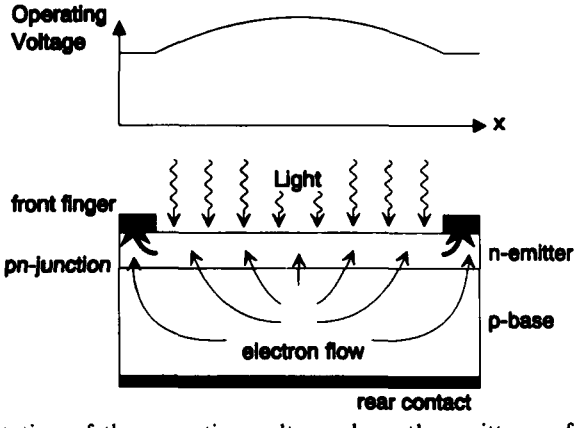

Figure 1. Schematic representation of the operating voltage along the emitter surface and the two-dimensional electron flow in the base of n^+pp^+ silicon solar cells resulting from the large finger spacing and the limited emitter sheet conductivity

ONE-DIMENSIONAL MODELLING OF EMITTER SHEET RESISTIVITY EFFECTS

Figure 2 shows a schematic view of the n^+pp^+ silicon solar cell to be investigated in this work. The high-efficiency features of this cell structure are a 200–300 μm thick high-lifetime p-type silicon substrate, a passivating SiO_2 layer on the front surface, a full-area 'back-surface field' (BSF) p^+ diffusion, a lightly diffused n^+ emitter and additional heavy n^{++} diffusions below the front metal fingers. The effects to be described, however, will be important in any device with high carrier lifetime and reasonable rear surface passivation.

Simple 1D model

If the light-generated minority carrier flow from the base into the emitter is assumed to be uniform, as indicated in Figure 2, a 1D treatment of ohmic emitter losses for the case of rectangular cells with parallel metal grid lines gives[6]

$$P_{\text{sheet}} = \frac{1}{12} \cdot \frac{J_{\text{mpp}}}{V_{\text{mpp}}} \rho_s s^2 \tag{1}$$

where P_{sheet} is normalized to the cell output power, ρ_s is the emitter sheet resistivity (in $\Omega\,\square^{-1}$), s is the spacing of the metal fingers and J_{mpp} and V_{mpp} are the current density and the voltage at the maximum power point, respectively. The normalized shading losses associated with the metal fingers are[6]

$$P_{\text{shade}} = \frac{w}{s} \tag{2}$$

where w is the shading width of the fingers. The shading losses decrease linearly with increasing finger spacing s, while the resistive emitter losses increase with the square of s. Thus, the optimum front finger spacing predicted by this simple 1D model is

$$s_{\text{opt}} = \sqrt[3]{\frac{6wV_{\text{mpp}}}{\rho_s J_{\text{mpp}}}} \tag{3}$$

This formula neglects contact resistance losses and resistive losses in the third dimension along the metal

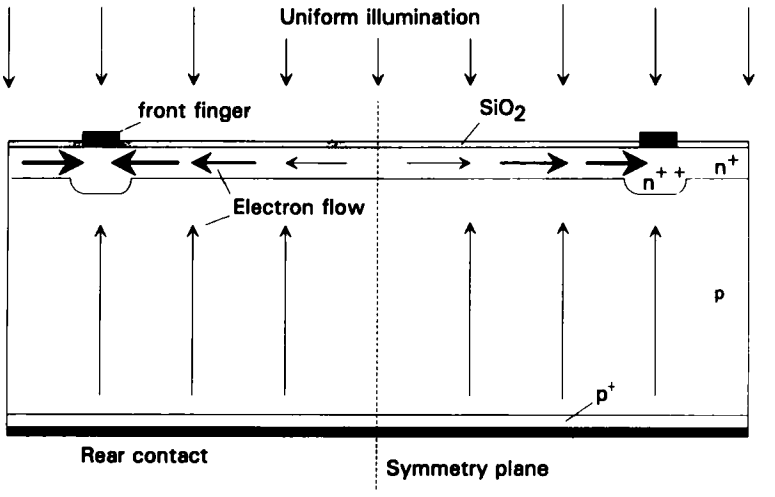

Figure 2. Two-dimensional schematic view of the n^+pp^+ silicon solar cell under investigation and the linear electron flow in emitter and base assumed by one-dimensional theory

fingers, although these can readily be incorporated at the same level of approximation.[6] However, these losses are neglected in this work.

For many years, 1D computer modelling has successfully been used for the optimization of design parameters of silicon solar cells.[7–9] In the simplest approach, 1D models are used to determine the I–V characteristics of a 1D solar cell along a vertical line between the two metal fingers in Figure 2. Subsequently, the sum of ohmic emitter losses and finger shading losses of the cell structure of Figure 2 is calculated from this I–V curve using Equations (1) and (2) and subtracted from the maximum power output. This method allows for a rough estimation of the impacts of emitter sheet resistivity and metal finger shading on cell I–V characteristics.

Extended 1D model

For a more accurate determination of cell I–V characteristics, recombination losses at the front metal fingers have to be considered. In order to include a first-order approximation of these losses on the basis of 1D theory, one can follow a '*pseudo two-dimensional*' (P2D) approach by dividing the total cell into two subcells (an illuminated diode and a non-illuminated fully metallized forward-biased diode in parallel) and assuming a *vertical* minority carrier flow in the emitter and the base and a *constant* operating voltage along the emitter surface. Thus, if the two diodes are treated as completely independent, the resulting saturation current of the total solar cell is given by

$$J_0(F_m) = F_m J_{o.dark} + (1 - F_m) J_{o.light} \tag{4}$$

where F_m is the metallized fraction of the front surface and $J_{o.dark}$ and $J_{o.light}$ are the saturation currents of the shaded and illuminated diode, respectively. Both saturation currents as well as the photocurrent J_L of the illuminated cell can either be calculated analytically[10,11] or numerically.[9] The resulting I–V curve of the total cell is then calculated analytically using, for instance, the one-diode model equation

$$J(V) = J_o(F_m)\left[\exp\left(\frac{V - JR_s}{nV_t}\right) - 1\right] + \frac{V - JR_s}{R_{sh}} - J_L \tag{5}$$

where R_s and R_{sh} are the series and shunt resistance of the cell, n is the diode ideality factor, V_t is the thermal voltage and J_L is the light-generated photocurrent density. From this implicit I–V equation, all relevant electrical parameters (open-circuit voltage V_{oc}, short-circuit current density J_{sc}, fill factor FF, maximum power power MPP) of the cell can be determined numerically. In the last step, as in the case of the simple 1D model, the ohmic emitter losses are calculated using Equation (1) and subtracted from the calculated maximum power output to obtain the final power output

$$P_{out} = J_{mpp} V_{mpp} - P_{sheet} \tag{6}$$

As neither the open-circuit voltage nor the short-circuit current are affected by resistive emitter losses, useful *analytical* expressions describing the dependence of J_{sc} and V_{oc} on the metallization fraction F_m can be derived from this P2D approach:

$$J_{sc}(F_m) = J_{sc.max}(1 - F_m) \tag{7a}$$

$$V_{oc}(F_m) = V_{oc.max} - nV_t \ln\left[\frac{1 + F_m(a - 1)}{1 - F_m}\right] \tag{7b}$$

where $J_{sc.max}$ and $V_{oc.max}$ are the short-circuit current density and the open-circuit voltage obtained for very small metallization fractions, respectively, while the constant a is the ratio of the saturation currents of the dark and illuminated diode: $a \equiv J_{o.dark}/J_{o.light}$. Equation (7b) is obtained from Equations (4) and (5), using the standard expression $V_{oc} = nV_t \ln(J_{sc}/J_o)$ for the open-circuit voltage. The increase of J_{sc} with decreasing F_m in Equation (7a) is solely due to reduced shading losses. The expression for the open-circuit voltage is more complicated, as V_{oc} depends on shading losses (via J_{sc}) as well as metal contact recombination (via J_o).

It should be noted that the P2D model is not self-consistent. As mentioned above, the model assumes a constant operating voltage along the emitter surface while the I–V characteristics of the cell are calculated. Conversely, in the calculation of the resistive emitter losses, a voltage drop along the emitter surface is implicitly assumed, leading to the power loss P_{sheet} of Equation (1) when a current is generated by the cell. In spite of this inconsistency, the P2D approach gives useful predictions of solar cell I–V characteristics using 1D theory. The usefulness of this P2D concept for the determination of optimum emitter parameters of silicon solar cells has recently been demonstrated.[12]

The accuracy of the P2D approach is high as long as the assumption of a constant operating voltage along the emitter surface is reasonably fulfilled. As this is only the case for closely spaced front fingers and/or small emitter sheet resistivity, considerable deviations from exact 2D simulations are expected if the P2D method is applied to high-efficiency silicon solar cells.

TWO-DIMENSIONAL NUMERICAL MODELLING OF SILICON SOLAR CELLS

Numerical solution of the normal semiconductor equations, a set of three non-linear partial differential equations, requires the introduction of a spatial grid. The grid is then used to discretize the equations, resulting in $3N$ non-linear equations that satisfy the appropriate boundary conditions, where N is the number of grid points. A linearization procedure leads to $3N$ linear equations that have to be solved repeatedly, resulting in values of the physical quantities (like carrier concentrations and current densities) at each grid point. These values are then used to calculate observable quantities like terminal currents. In order for the numerical procedure to produce meaningful results, the physically active device regions must be resolved properly by the simulation grid. This means that in regions of the device where relevant quantities (e.g. doping concentration or carrier generation rates) vary strongly, a high grid point density is required. In solar cells, such regions are the emitter, the back-surface field and the shadow boundary underneath the opaque front contacts, where grid point separations of less than 0.2 μm are typically required. Another difficulty arises from the fact that the simulation domain required to model a high-efficiency silicon solar cell is huge compared to the size of the smallest features. Typical cells are 200–300 μm thick and exhibit a finger spacing of about 1 mm. For symmetry reasons, the minimum simulation domain is given by the thickness of the cell and half the finger spacing (Figure 3). This cannot be reduced further, because, owing to the extreme diffusion lengths (>1 mm), the whole volume of high-efficiency silicon solar cells is electronically active. If the density of grid points were uniform throughout the device, several million grid points would be required to model such a cell.

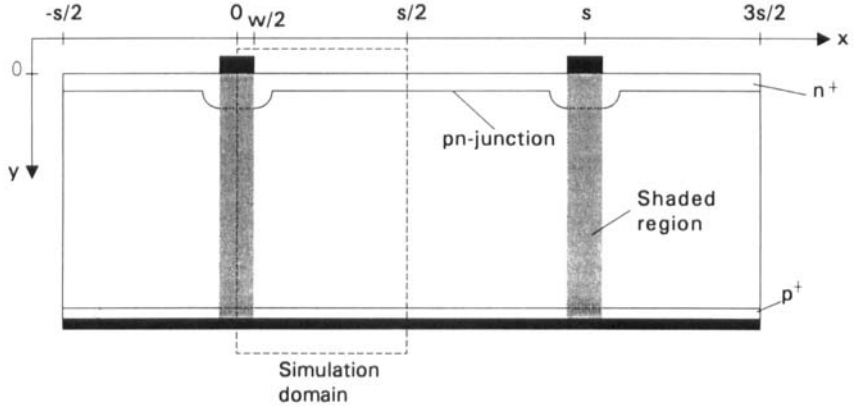

Figure 3. Simulation domain used for the numerical two-dimensional simulations of silicon solar cells. Symmetry arguments limit the simulation domain to the area given by the cell thickness and half the finger spacing

The size of the simulation grid is one of the most critical factors determining the feasibility of numerical modelling. The amount of computer memory required to solve the system of linear equations arising from the discretization of the semiconductor equations in d dimensions is approximately proportional to $(3N)^{(d+2)/3}$ if direct solvers are used, while for iterative solvers memory requirements are linear in the number of grid points.[13] For instance, a 2D simulation with 10^5 mesh points will require about 1500 Mbytes of computer memory when direct solvers are used, and about 150 Mbytes for iterative methods. It is therefore essential to keep the grid size as small as possible by adapting the grid to the device in such a way that the point density is sufficiently high where needed and sufficiently low where the physical quantities vary only slightly. In the less active device regions, grid point separations of up to 20 μm are often sufficient.

Such intensive control over the simulation grid is not supported by most device simulators, which will often produce 10^5 or more grid points when applied to a typical silicon solar cell, hence making extensive supercomputer access essential even for 2D simulations. Furthermore, these grids tend to contain many obtuse triangles, even one of which can lead to large spikes in the solution,[14] which may completely destroy the accuracy of the simulation. In contrast, the ETH grid generator produces grids that are, by construction, free of obtuse triangles.[15] This program, which provides very good control over the grid density, allowed us to model high-efficiency silicon solar cells with simulation grids of only 3000–10 000 points (Figure 4). This is small enough to perform the simulations on a Sun SPARC-2 workstation with 64 Mbytes of memory, which will support grid sizes of up to 15 000 points using direct solvers or 40 000 points with iterative solvers.

The above problems are aggravated by the fact that the linearized equations arising in semiconductor device simulations are generally very ill-conditioned, making them extremely hard to solve by iterative methods. Most of the usual iterative methods, even in conjunction with preconditioning techniques, turn out to be unsuitable.[13] Improved convergence behaviour is one of the main strengths of the ETH software package that makes it suitable for large-scale device simulations.[16,17] Last, but not least, Simul comes with the 2D/3D visualization tool Picasso,[18] which is extremely valuable for detecting and solving possible problems arising during the simulations and for understanding the operating conditions of the simulated devices. For all these reasons, we found the ETH simulator Simul to be well suited for our investigations and anticipate that we will be able to perform even 3D simulations of the rear point contacts of the highest-efficiency one-sun silicon solar cells made at the University of New South Wales (UNSW).[2]

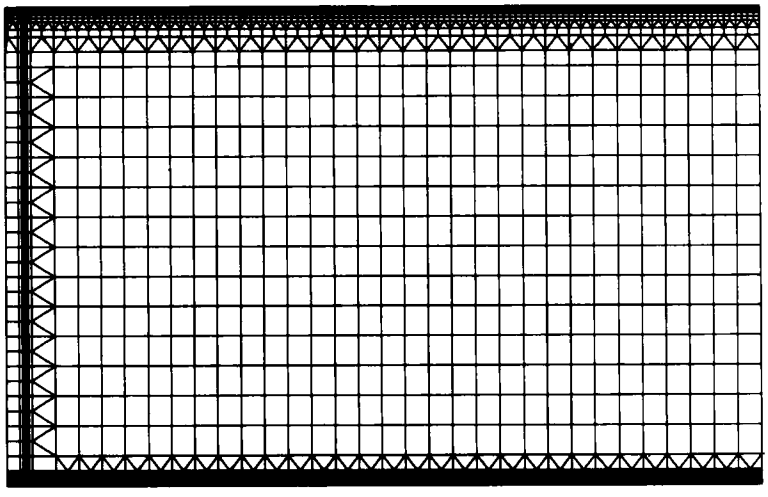

Figure 4. Typical simulation mesh for a 250 μm deep and 400 μm wide simulation domain of an n^+pp^+ silicon solar cell. A single metal finger sits on the top left corner, while the right end of the plot coincides with the centre between two front metal fingers (see Figures 2 and 3). This mesh consists of 4203 points

RESULTS

As qualitatively discussed above (Figure 1), for widely spaced metal fingers, the minority carrier flow in the base is expected to deviate from simple 1D theory. In order to quantify the effect for a typical high-efficiency device, we have used Simul to model a 250 μm thick n^+pp^+ silicon BSF solar cell. Table I summarizes the cell parameters and specifies the selected physical models. The optimum profile parameters for the n^+ and n^{++} phosphorus diffusions agree well with experimental high-efficiency devices at UNSW, as well as with modelling results.[12] The p^+ profile results from a parameter study with the one-dimensional solar cell simulation program PC-1D.[19] In order to eliminate possible 2D effects arising from the rear contacts, a fully metallized rear surface is assumed. The substrate Shockley-Read-Hall (SRH) low-injection lifetime of 2 ms represents the highest quality 1 Ωcm float-zone (FZ) silicon and results in a bulk diffusion length of about 2.5 mm. To gain insight into the effects introduced by the wavelength of the light, simulations are performed for blue (400 nm), infrared (1000 nm) and Air Mass 1.5 (AM1.5) illumination. In each case the light intensity is adjusted so that for very large finger spacings a short-circuit current density of about 41 mA cm^{-2} is obtained, which is the typical AM1.5 value for high-efficiency silicon solar cells.

Illumination with *long wavelength* results in a nearly uniform carrier generation in silicon solar cells and large minority carrier concentrations near the rear surface. Figure 5 shows the calculated electron flow pattern in the base of a 250 μm deep n^+pp^+ silicon solar cell for infrared illumination (1000 nm) and one-sun maximum power point conditions. The half finger spacing is 400 μm and 800 μm, respectively, for the two cases shown. It should be noted that the electron current density is a vector. For visualization reasons, we have chosen to use grey shading to indicate the magnitude of the current density, while the flow lines in Figure 5 show the path along which the electrons actually move (i.e. the direction of the current density vector). The 2D simulations show that the electron flow in the base is indeed not purely vertical, but has a significant lateral component, which results from the fact that the electron concentration is highest near the rear surface, halfway between the front metal fingers (lower right-hand corner in Figure 5). The horizontal current component is particularly large for electrons generated near the rear surface. These electrons initially diffuse laterally along the rear surface, until they diffuse upwards to be collected by the emitter. Consequently, a significant fraction of the electron current that otherwise would have to be transported by the emitter flows through the base of the cell. As expected, the wider the cell the stronger the 2D effect. However, owing to the enhanced electron path length in the base,

Table I. Parameters of the silicon solar cell under investigation and selected physical models of Simul

Cell structure	n^+pp^+ silicon BSF solar cell, planar front and rear surface, fully metallized rear surface
Substrate	p-type FZ silicon, 1.0×10^{16} cm^{-3} (1.37 Ω·cm)
Cell thickness	250 μm
p^+ BSF diffusion	Gaussian, $N_s = 1 \times 10^{19}$ cm^{-3}, depth = 5.0 μm, $\rho_s = 45$ Ω □$^{-1}$
n^+ diffusion	Gaussian, $N_s = 5 \times 10^{18}$ cm^{-3}, depth = 1.0 μm, $\rho_s = 200$ Ω □$^{-1}$
n^{++} diffusion	Gaussian, width = 6.2 μm, depth = 2 μm, $\rho_s = 11$ Ω □$^{-1}$
Front grid	Parallel fingers, metal/silicon interface 3 μm, shading width 20 μm
Finger spacing	Variable
Contact resistance	Neglected
Illumination	Spatially uniform, 400 nm or 1000 nm or AM1.5
Cell temperature	300 K
Shockley-Read-Hall recombination	Low-injection lifetime $\tau_0 = 2$ ms, midgap traps, SRH lifetime independent of electric fields
Surface recombination model	$S_{metal} = \infty$, $S_{oxide} = 1000$ cm s^{-1}, flatband conditions at surface
Mobility[20]	Doping dependent, no carrier–carrier scattering
Radiative recombination	Neglected
Auger recombination[21,22]	$C_n = 3.338 \times 10^{-31}$ cm^6 s^{-1}, $C_p = 1.028 \times 10^{-31}$ cm^6 s^{-1} at 300 K, no trap-assisted Auger recombination
Bandgap narrowing model[23]	Bennett-Wilson (BW)
Intrinsic carrier density model[24]	Modified BW with n_i (300 K) = 1.00×10^{10} cm^{-3}

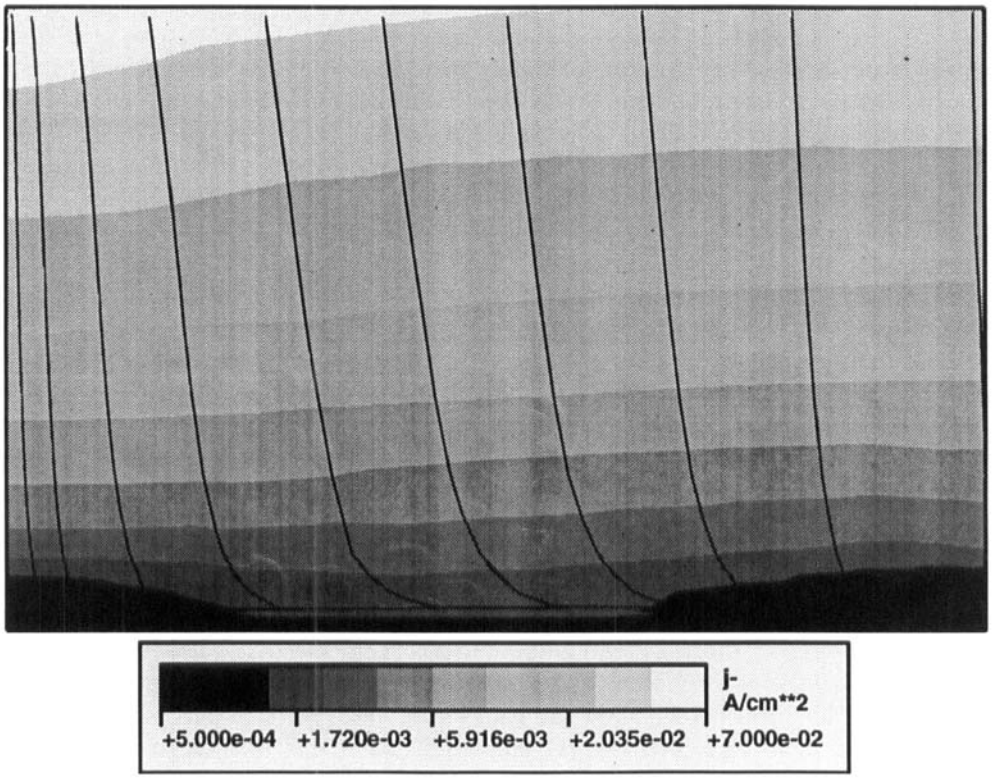

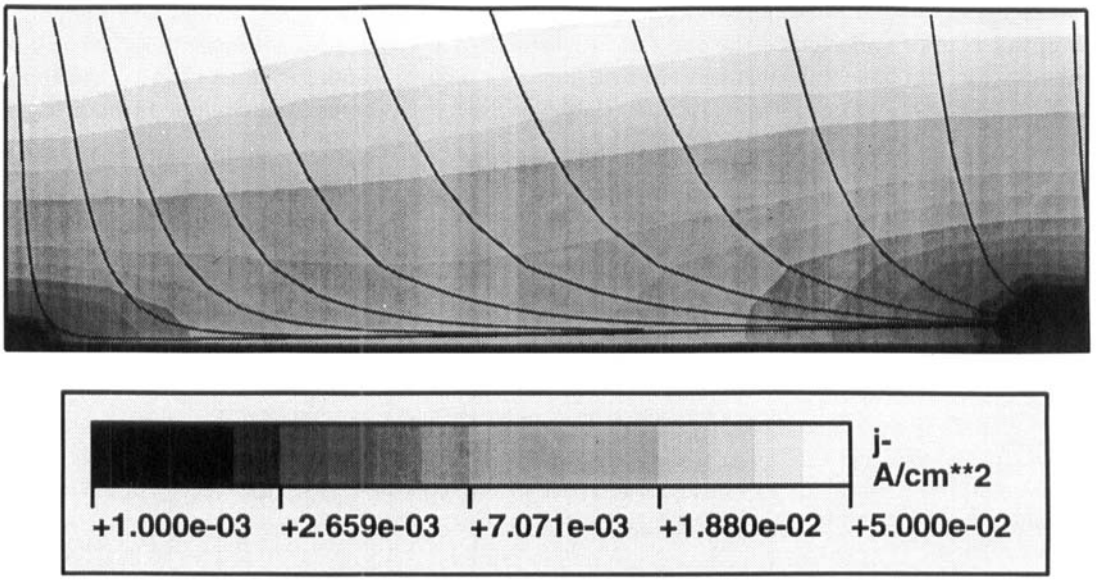

Figure 5. Calculated electron current density and electron flow lines in the base of n^+pp^+ silicon solar cells under *infrared illumination* (1000 nm) and one-sun maximum power point conditions. The width of the simulation domain (i.e. half the finger spacing) is 0.4 mm (top) and 0.8 mm (below), while the thickness of the cell is 250 μm in both cases. The flow lines indicate the direction of the electron current at any point within the device (the electrons diffuse upwards along the flow lines), while the background shading shows the corresponding magnitude (darkest colours correspond to *smallest* currents). For the definition of the simulation domain see Figures 2–4

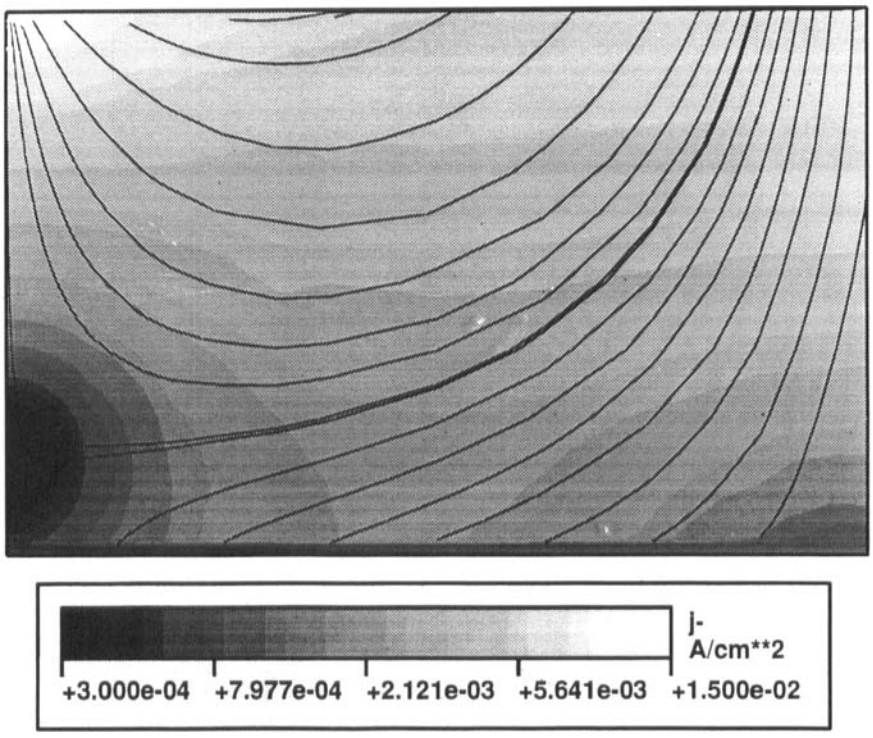

Figure 6. Two-dimensional electron flow resulting from *blue illumination* (400 nm) at maximum power point conditions (half finger spacing = 0.4 mm; see Figure 5 for interpretation of flow lines and shading)

this 2D effect is only beneficial for solar cell efficiency if the electron diffusion length is much larger than half the finger spacing.

In contrast, *short-wavelength* light is completely absorbed within the emitter of silicon solar cells. In Figure 6, the electron flow pattern in the n^+pp^+ solar cell of Table I resulting from 400 nm illumination is plotted for maximum power point conditions. The 2D simulation shows that a considerable fraction of the electrons that have been light-generated in the far right emitter region do not flow right through the emitter to be collected by the metal finger in the top left corner, but are injected into the base. This forward-injection behaviour results from the operating voltage profile along the emitter surface. A major fraction of the base-injected electrons recombines in the base or at the rear surface, a phenomenon that, in principle, can be understood from 1D theory. Interestingly, however, and in sharp contrast to 1D theory, a significant fraction of the base-injected electrons does *not* recombine in the base or at the rear surface, but is redirected towards the emitter and finally recollected by the emitter region near the metal finger.

In the case of *AM1.5 illumination* (Figure 7), the effects discussed above are combined to produce an even more complex current flow pattern than in the case of infrared or blue illumination. Compared to long-wavelength illumination, as a result of the shorter wavelengths in the AM1.5 spectrum, the generation profile is considerably shifted towards the front surface and the maximum electron concentration in the base occurs close to the p-n junction, in the central region between two front fingers (top right corner in Figure 7). This localized maximum of the electron concentration is the reason for the remarkable current flow in the top right base region of Figure 7. A comparison of the minority carrier flow patterns in Figure 7 and Figure 2 reveals that 1D models grossly oversimplify the operating conditions of high-efficiency silicon solar cells.

As a result of the 2D current flow in the base, the electron current density flowing from the base into the emitter is not uniform but depends strongly on the distance from the metal finger. Figure 8 shows

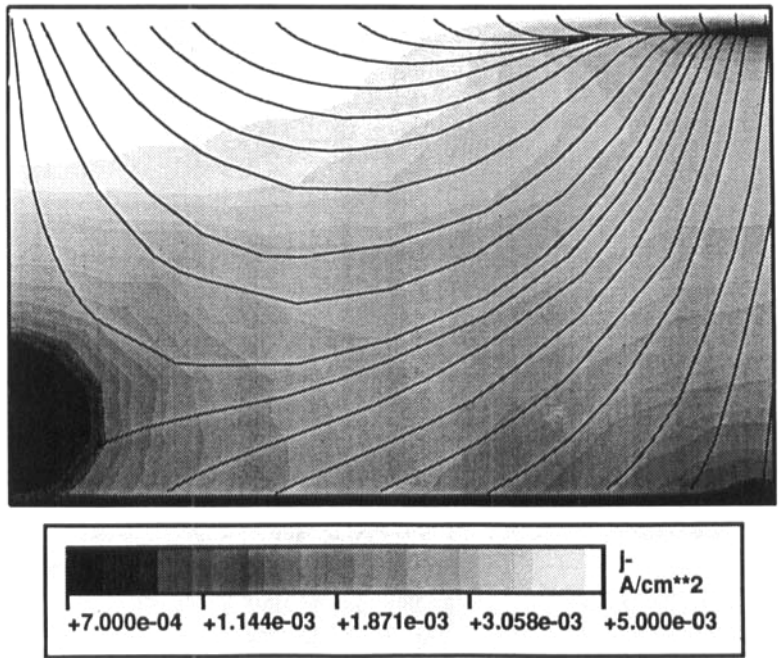

Figure 7. Calculated electron current density in the base of a 250 μm deep n^+pp^+ silicon solar cell under *AM1.5 illumination* (maximum power point, half finger spacing = 0.4 mm; see Figure 5 for interpretation of flow lines and shading)

the effect for the cell dimensions and operating conditions of Figure 7, which lead to a voltage drop of 5.5 mV along the emitter surface. As a result of this voltage profile, the current density entering the emitter in the right half of the simulation domain is reduced by up to 30% compared to the constant current density of about 15 mA cm^{-2} that is predicted by 1D models, while it is correspondingly larger in the left half. This plot implies that in more than half of the emitter the total *lateral* current is significantly smaller than is assumed by 1D models.

In Figure 9, the 2D results for the AM1.5 parameters short-circuit current, open-circuit voltage, power output and fill factor of the n^+pp^+ silicon solar cell of Table I are plotted as a function of the front finger spacing. The width of the metal/silicon interface is 3 μm, while the shading width of the metal finger is assumed to be 20 μm. These values are based on experimental one-sun UNSW devices. Initially, the metal fingers are metallized in a vacuum evaporation system, resulting in finger widths of 3 μm and finger heights of less than 0.2 μm. Subsequently, the fingers are electroplated with silver to a height of 8–10 μm in order to minimize ohmic losses in the fingers. The experimental final finger shape can be approximated by a half-circle and results in an effective shading width of about 20 μm.[25]

The dashed line in Figure 9(a) compares the 2D results for the short-circuit current J_{sc} with the simple analytical 1D expression of Equation (7a). For this comparison, the 1D current was normalized to the 2D current obtained for *large* finger spacings (3 mm), because for widely spaced fingers the impact of recombination in the shaded device regions on J_{sc}—which is not included in 1D models—is minimized and 1D and 2D models give similar results. The excellent agreement between the two models indicates that the dependence of J_{sc} on finger spacing is fully determined by the shading losses associated with the front metal fingers (see Equation (7a)). Thus, current losses at the front metal contacts or in the underlying heavily doped n^{++} region (see Figure 2) are negligible in the investigated cell. This is plausible from the cell parameters of Table I, indicating that the distance between the shadow boundary and the edge of the heavily doped n^{++} region (7 μm) is much larger than the emitter minority carrier diffusion length. Furthermore, for the investigated range of finger spacings (<3 mm), the 2D simulations do not

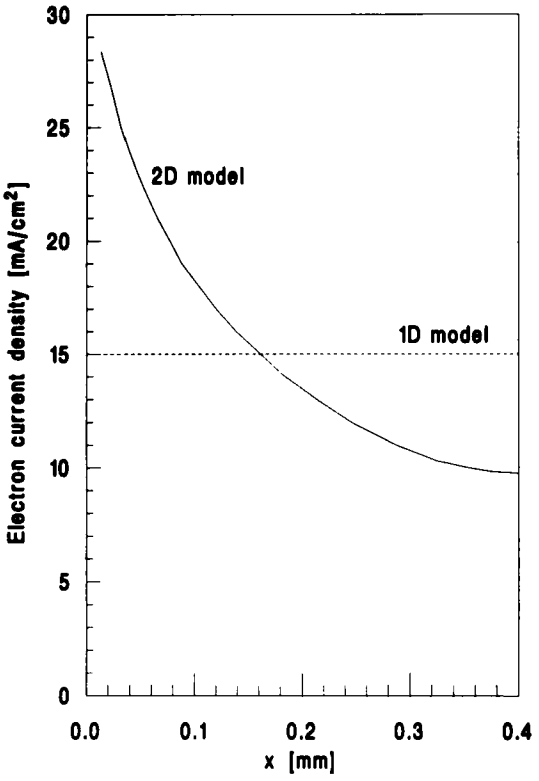

Figure 8. Light-generated electron current density flowing from the base into the emitter as a function of the distance from the top left metal finger (AM1.5 illumination, maximum power point, half finger spacing = 0.4 mm)

yet show any decrease of J_{sc} due to current losses in the base (owing to recombination losses in the base, 2D theory predicts a decrease of J_{sc} if the half-finger spacing is larger than the base diffusion length, see discussion of Figure 5).

Similarly, in Figure 9(b), the 1D expression for the open-circuit voltage (Equation (7b)) is compared with the 2D simulations. The 1D curves are again normalized to the 2D result for large finger spacings, because for widely spaced fingers the impact of recombination in the shaded regions of the cell is minimized. Excellent agreement between 1D and 2D models is obtained if the parameter a in Equation (7b) is assumed to be 1.63, which means that the saturation current density of the fully metallized diode is about 63% larger than that of the illuminated diode. Owing to the relatively small value of a, the open-circuit voltage does not improve significantly once the finger spacing exceeds 1 mm. This indicates that recombination at the front metal fingers does not limit the AM1.5 efficiently of the modelled cell.

Figure 9(c) compares the dependence of power output on front finger spacing according to 1D and 2D theory. Here, the 1D curve was normalized to the 2D result for *small* finger spacings (0.25 mm), because in this case 2D effects in the cell as well as resistive emitter losses are negligible and—owing to nearly identical values for J_{sc} and V_{oc} (see Figures 9(a) and 9(b))—1D and 2D models give similar results. The variation of the 1D curve with finger spacing was calculated using the dashed lines of Figure 9(a) and (b) for the dependence of J_{sc} and V_{oc} on finger spacing (for V_{oc}, the dashed curve labelled $a = 1.63$ was used) and Equation (1) for the emitter sheet resistivity losses. Compared to 1D theory, the 2D simulations show a slightly larger optimum finger spacing (1.1 mm instead of 1.0 mm), a wider range for the optimum finger spacing (0.9–1.4 mm as opposed to the 0.9–1.1 mm range seen by 1D theory) and a significantly reduced decrease of power output with increasing finger spacing. This behaviour results from the reduced ohmic emitter losses correlated with the 2D current flow in the base of the cell (see Figures 7 and 8). Under low-injection conditions, the minority carrier flow in the base is driven by

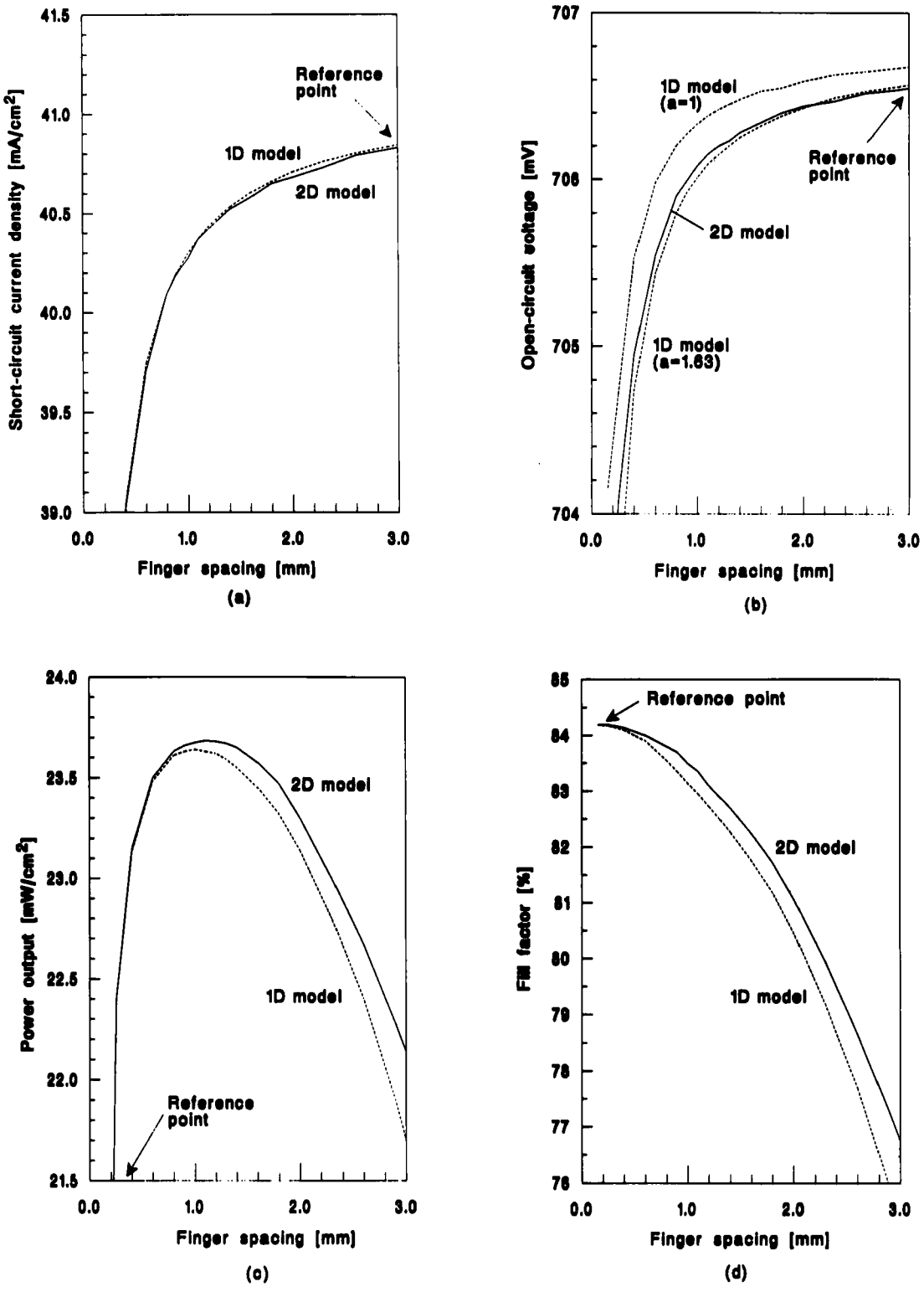

Figure 9. Calculated AM1.5 parameters (a) short-circuit current, (b) open-circuit voltage, (c) power output and (d) fill factor of the n^+pp^+ silicon solar cell of Table I as a function of the front finger spacing. The dashed lines show the predictions of the extended one-dimensional model

diffusion forces (and not by electric fields) and therefore the additional current flow in the base does not increase ohmic device losses.

Figure 9(c) shows that, despite the clearly multidimensional current flow in the investigated high-efficiency solar cell, the 1D theory still does a remarkably good job of predicting the performance and the optimum front finger spacing under one-sun illumination. For one-sun cells with less ideal diffusion lengths, a 1D treatment is fully adequate.

The voltage drop along the emitter surface increases with light intensity. Consequently, the 2D effects in the base of silicon solar cells and the reduced impact of resistive emitter losses on cell efficiency are more pronounced under concentrated sunlight. Figure 10(a) summarizes the calculated optimum finger spacing of the solar cell of Table I as a function of light intensity. The calculations assume the same finger geometry as in the one-sun simulations of Figure 9 (i.e. the width of the metal/silicon interface is 3 μm and the effective shading width of the fingers is 20 μm). The solid line represents the 2D results, while the dashed line again is calculated with the extended 1D model. The optimum front finger spacing is found to decrease with increasing light level; however, the dependence is significantly reduced at large light intensities. This 'saturation effect' results from the fact that at high concentrations the magnitude of the lateral current in the emitter is small compared to the lateral current in the base. Furthermore, the plot shows that at low light intensities the finger spacing predictions of the 1D model agree well with the 2D results, while at higher concentrations the deviations become more pronounced (e.g. 10%

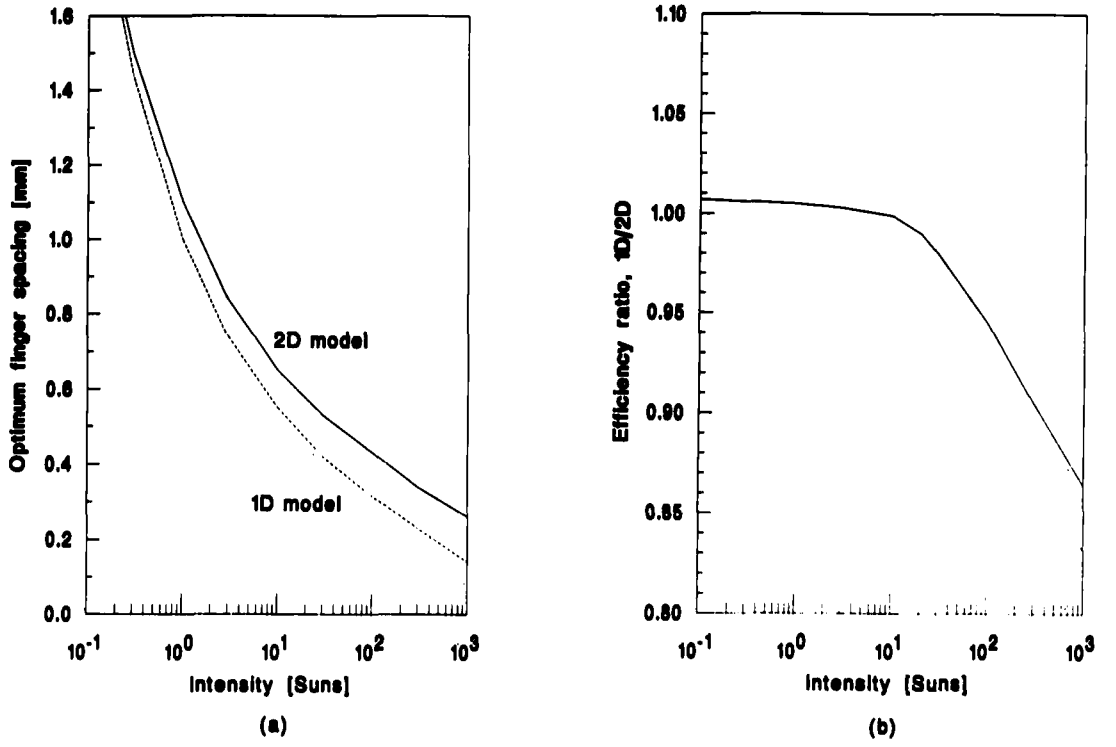

Figure 10. Impact of light intensity on the optimum front finger spacing (a) and the ratio of the obtainable maximum efficiencies (b) of the n^+pp^+ silicon solar cell of Table I obtained from one-dimensional and two-dimensional simulations. The calculations assume a constant finger geometry optimized for one-sun applications (i.e. the finger width is independent of light intensity) and do not take into account metal contact resistance and ohmic losses along the metal fingers

deviation at 1 sun, compared to 32% at 100 suns). Figure 10(b) compares the maximum cell efficiencies obtained from 1D and 2D simulations as a function of light concentration. The deviations are negligible below 10 sums, while at higher light levels the 1D simulations, owing to the overestimated resistive emitter losses, show significantly smaller efficiencies.

It should be noted that the results of Figure 10 cannot be applied directly to experimental concentrator devices because contact resistance losses at the metal/silicon interface, as well as resistive losses along the front fingers (i.e. along the third dimension), are neglected and the simulations are based on a one-sun finger geometry. Experimentally, front contact resistance has not been found to be a problem in n^+p silicon concentrator solar cells.[26] A slightly heavier n^{++} diffusion below the metal contacts and a metal/silicon interface about 3–5 times wider will keep contact resistance losses at tolerable levels for light concentrations as high as several hundred suns. The effect of resistance losses due to current flow along fingers in the third dimension will tend to reduce the optimum finger spacing below the predictions of Figure 10 by an amount dependent on the finger length and the light intensity.[27]

The differences between 1D and 2D models in Figure 10 strongly depend on the design parameters of the cell under investigation (e.g. the emitter sheet resistivity and the shading width of the metal fingers, see Equation (3)). An earlier 2D investigation of silicon concentrator solar cells at Purdue University predicted no difference between 1D and 2D models for light concentrations up to 400 suns.[28]

CONCLUSIONS

In this work, state-of-the-art 2D numerical semiconductor device simulation tools are applied to bifacially-contacted silicon solar cells of practical dimensions in order to investigate the 2D effects arising from the front metal grid line spacing and the emitter sheet resistivity. The 2D simulations show that for typical front finger spacings of high-efficiency silicon solar cells the minority carrier flow in the base deviates strongly from the purely linear flow assumed by 1D theory. This 2D effect is a direct consequence of the limited emitter sheet conductivity and the large finger spacing, leading to a significant drop in the operating voltage along the emitter surface when a current is generated by the cell.

As a result of the 2D minority carrier flow in the base, the current density in the central emitter regions is significantly reduced, leading to smaller emitter sheet resistance losses than predicted by conventional 1D theory. In high-efficiency silicon solar cells, this 2D effect leads to an increased optimum front finger spacing and a reduced impact of finger spacing on cell efficiency, compared to 1D theory. In the case of AM.15 illumination, the 2D simulations show an optimum finger spacing of about 1.1 mm for high-efficiency silicon solar cells, which is only slightly above the 1.0 mm predicted by 1D theory. The optimum finger spacing of silicon concentrator solar cells, however, is found to be significantly larger than suggested by 1D theory.

The 2D simulations presented in this work considerably improve the general understanding of internal device physics of high-efficiency silicon solar cells and reveal the limits of 1D models for the simulation of these devices.

Acknowledgements

This work was partly funded by a Research Grant from the Australian Research Council. The Centre for Photovoltaic Devices and Systems is supported by the Australian Research Council's Special Research Centres Scheme and Pacific Power. One of the authors (A.G.A.) gratefully acknowledges the support of a Feodor Lynen Fellowship provided by the German Alexander von Humboldt Foundation and fruitful discussions with Dr Andrew Blakers, Australian National University, Canberra. Finally, we would like thank Prof. Dr Wolfgang Fichtner from ETH Zurich for granting access to the latest versions of Simul, and Kevin Kells and Ulrich Krumbein of his group for their help with various problems encountered in the 2D simulations.

REFERENCES

1. R. A. Sinton, Y. Kwark, J. Y. Gan and R. M. Swanson, '27.5-Percent silicon concentrator solar cells', *IEEE Trans. Electron Devices Lett.* **EDL-7**, 567 (1986).
2. A. Wang, J. Zhao and M. A. Green, '24% efficient silicon solar cells', *Appl. Phys. Lett.* **57**, 602 (1990).
3. M. A. Green, 'Recent advances in silicon solar cell performance', *Proc. 10th European Communities Photovoltaic Solar Energy Conference, Lisbon, Portugal, 1991*, p. 250, Kluwer, Dordrecht, 1991.
4. Simul Manual, Integrated Systems Lab., ETH Zurich, Switzerland, 1992.
5. U. Krumbein and W. Fichtner, *Numerical Simulation of Optical Carrier Generation*, Technical Report 91/22, Integrated Systems Lab., ETH Zurich, Switzerland, 1991.
6. M. A. Green, *Solar Cells*, University of New South Wales, PO Box 1, Kensington, NSW 2033, Australia, 1982.
7. J. R. Hauser and P. M. Dunbar, 'Performance limitations of silicon solar cells', *IEEE Trans. Electron Devices* **ED-24**, 305 (1977).
8. J. L. Gray and R. J. Schwartz, 'Why don't we have a 30% efficient silicon solar cell', *Proc. 18th IEEE Photovoltaic Specialists Conference, Las Vegas, USA, 1985*, p. 568, IEEE, New York, 1985.
9. P. A. Basore, D. T. Rover and A. W. Smith, 'PC-1D: enhanced numerical solar cell modeling', *Proc. 20th IEEE Photovoltaic Specialists Conference, Las Vegas, USA, 1988*, p. 389, IEEE, New York, 1988.
10. S. M. Sze, *Physics of Semiconductor Devices*, 2nd Edn, Wiley, New York, 1981.
11. J. S. Park, A. Neugroschel and F. A. Lindholm, 'Systematic analytical solutions for minority-carrier transport in semiconductors with position-dependent composition, with application to heavily doped silicon', *IEEE Trans. Electron Devices* **ED-33**, 240 (1986).
12. A. G. Aberle, W. Warta, J. Knobloch and B. Voss, 'Surface passivation of high efficiency silicon solar cells', *21st IEEE Photovoltaic Specialists Conference, Orlando, USA, 1990*, p. 233, IEEE, New York, 1990.
13. C. Pommerell and W. Fichtner, 'Memory aspects and performance of iterative solvers', *Proc. 2nd SIAM Copper Mountain Conference on Iterative Methods*, Copper Mountain, USA, 1992, SIAM, Philadelphia, 1992. To appear in *SIAM J. Sci. Stat. Comput.* (1994).
14. M. R. Pinto, C. S. Rafferty and R. W. Dutton, *PISCES-2: Poisson and Continuity Equation Solver*, Stanford University, USA, 1984.
15. S. Müller, K. Kells and W. Fichtner, 'Automatic rectangle-based adaptive mesh generation without obtuse angles', *IEEE Trans. CAD* **CAD-11**, 855 (1992).
16. G. Heiser, C. Pommerell, J. Weis and W. Fichtner, 'Large-scale device simulation: algorithms, computer architectures, results', *IEEE Trans. CAD* **CAD-10**, 1218 (1991).
17. A. Liegmann and W. Fichtner, *The Application of Supernodal Factorisation Algorithms for Structurally Symmetric Linear Systems in Semiconductor Device Simulation*, Technical Report 92/17, Integrated Systems Lab., ETH Zurich, Switzerland, 1992.
18. M. Westermann, *Picasso 2.1 User's Guide*, Integrated Systems Lab., ETH Zurich, Switzerland, 1992.
19. A. G. Aberle, 'Untersuchungen zur Oberflächenpassivierung von hocheffizienten Silicium-Solarzellen', PhD Thesis, University of Freiburg, Germany, p. 74, 1991.
20. G. Masett, M. Severi and S. Solmi, 'Modelling of carrier mobility against carrier concentration in arsenic-, phosphorus- and boron-doped silicon', *IEEE Trans. Electron Devices* **ED-30**, 764 (1983).
21. L. Huldt, N. G. Nilsson and K. G. Svantesson, 'The temperature dependence of band-to-band Auger recombination in silicon', *Appl. Phys. Lett.* **35**, 776 (1979).
22. W. Lochmann and A. Haug, 'Phonon-assisted Auger recombination in Si with direct calculation of the overlap integrals', *Solid State Commun.* **35**, 553 (1980).
23. H. S. Bennet and C. L. Wilson, 'Statistical comparisons of data on band-gap narrowing in heavily doped silicon: electrical and optical measurements', *J. Appl. Phys.* **55**, 3582 (1984).
24. A. B. Sproul and M. A. Green, 'Improved value for the silicon intrinsic carrier concentration from 275 to 375 K', *J. Appl. Phys.* **70**, 846 (1991).
25. A. W. Blakers, 'Shading losses of solar-cell metal grids', *J. Appl. Phys.* **71**, 5237 (1992).
26. J. Zhao, 'High efficiency silicon concentrator solar cells', PhD Thesis, University of New South Wales, Kensington, Australia, 1989.
27. P. A. Basore, 'Optimum grid-line patterns for concentrator solar cells under nonuniform illumination', *Sol. Cells* **14**, 249 (1985).
28. R. J. Schwartz, J. L. Gray and M. S. Lundstrom, *Report on High Intensity Solar Cells*, Report SAND84-7002, Sandia National Laboratories, USA, 1985.